THE JOURNAL OF PHYSICAL CHEMISTRY C
A JOURNAL OF THE AMERICAN CHEMICAL SOCIETY

pubs.acs.org/JPCC

Article

Inelastic Neutron Scattering Study of Magnetic Exchange Pathways in MnS

Published as part of The Journal of Physical Chemistry virtual special issue "Alexander Boldyrev Festschrift".

Judith K. Clark, Vincent Yannello, Anjana M. Samarakoon, Cyris Ross, Madeleine C. Uible, V. Ovidiu Garlea,* and Michael Shatruk*

Cite This: *J. Phys. Chem. C* 2021, 125, 16183−16190

Read Online

ACCESS | Metrics & More | Article Recommendations | Supporting Information

ABSTRACT: We report an investigation of the magnetic structure and magnetic exchange pathways in MnS via neutron scattering methods, aided by density functional theory (DFT) modeling. The material has been confirmed to undergo antiferromagnetic (AFM) ordering at 152 K, with the magnetic structure representing AFM stacking of ferromagnetic (FM) (111) planes of Mn magnetic moments. Correspondingly, the magnetic structure is described by a propagation vector $\boldsymbol{k}$ = (1/2, 1/2, 1/2), with the volume of the magnetic unit cell being 8 times larger than the volume of the nuclear unit cell. Analysis of inelastic neutron scattering (INS) data collected on a powder sample of MnS revealed that the next-nearest-neighbor magnetic exchange constant (J_2) exceeds the nearest-neighbor exchange constant (J_1) by more than 3 times, while in the case of MnO, which exhibits the same nuclear and magnetic structures as MnS, the J_2/J_1 ratio was reported to be below 1.5. Although for MnO the signs of both J_1 and J_2 indicated AFM exchange interactions, machine-learning INS data analysis in combination with DFT calculations suggests that the INS data collected on MnS are best described with $J_1 < 0$ and $J_2 > 0$, corresponding to FM and AFM exchange couplings, respectively. To achieve a satisfactory fit to the experimentally observed data, the Hamiltonian used to model the INS spectra also included the next-next-nearest-neighbor magnetic exchange constant (J_3). The best-fit model has been obtained with the values of the exchange constants J_1 = −0.27 meV, J_2 = 1.05 meV, and J_3 = −0.19 meV.

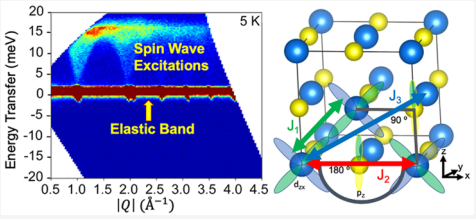

INTRODUCTION

Magnetic properties of manganese monochalcogenides have been thoroughly investigated for nearly a century. The stable forms of MnO and MnS exhibit the cubic NaCl-type structure. In 1939, the study carried out by Squire revealed antiferromagnetic (AFM) phase transitions in these compounds, with the ordering temperature (T_N) increasing with the increasing atomic number of chalcogen.[1] In fact, MnO was among the first materials for which the magnetic structure was determined by neutron powder diffraction.[2] Shull and coworkers demonstrated that the magnetic moments of Mn were ordered ferromagnetically (FM) within (111) planes, but the moments in adjacent (111) planes were coupled antiparallel to yield the overall AFM state (Figure 1). Despite these early studies, the knowledge of the exact magnetic structure of MnO had remained incomplete for more than 50 years, until Goodwin et al. conclusively established that the Mn moments in the AFM state are oriented parallel and antiparallel to the $[11\bar{2}]$ direction.[3] The magnetic moment was found to be 5.66 μ_B per Mn atom at 10 K.

In their seminal paper,[2] Shull et al. also suggested, based on the neutron diffraction patterns, that the isostructural MnS and MnSe possessed the same magnetic structures as that of MnO. This suggestion was confirmed a few years later for MnS,[4]

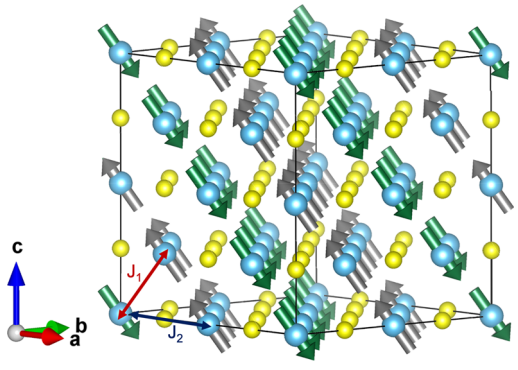

Figure 1. Magnetic structure of MnO and MnS. The alternating directions of the Mn moments in the (111) planes are indicated with different colored arrows. The J_1 (red) and J_2 (blue) magnetic exchange pathways are shown. Color scheme: Mn = light blue; O and S = yellow.

Received: April 1, 2021
Revised: June 29, 2021
Published: July 15, 2021

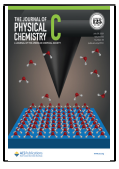

although the exact value of the Mn magnetic moment in the AFM ordered state was not reported. A study carried out by van der Heide et al. established the magnetic moment of 4.46 μ_B per Mn atom at 4.2 K,[5] while a recent work by Huang et al. reported a slightly higher value of ∼4.8 μ_B.[6] Thus, in comparison to the magnetic moment reported for MnO, the moment per Mn atom in MnS is notably smaller. This decrease can be attributed to the increased covalency of the Mn−X bonding, which also should affect the strength of magnetic exchange interactions. Despite the simplicity of their crystal structures, manganese monochalcogenides are important reference materials, since the knowledge of their magnetic parameters and magnetic exchange interactions can be used to understand the influence of covalency and delocalization of chemical bonding[7−9] on the magnetic properties and magnetic structures of related materials, e.g., more complex ternary and quaternary chalcogenides.[10−12]

Inelastic neutron scattering (INS) is a unique tool to probe magnetic exchange interactions in materials. It allows direct measurement of magnetic excitations in the energy−momentum space. For example, single-crystal INS measurements were used to determine the nearest-neighbor (NN) and next-nearest-neighbor (next-NN) magnetic exchange constants in MnO.[13,14] Interestingly, the J_1 constant, which describes the NN exchange interaction at d(Mn−Mn) ∼ 3.14 Å, turned out to be only slightly smaller than the J_2 constant, which describes the next-NN exchange interaction at d(Mn−Mn) ∼ 4.4 Å. The ratio J_2/J_1 = 1.15 indicates the effectiveness of the magnetic superexchange across the 180° Mn−O−Mn bridge (Figure 1). The higher-order exchange parameters had a negligible effect on the fit to the experimental INS data, but an additional fitting parameter had to be included to account for the slight rhombohedral distortion known to occur in MnO at lower temperatures.[15] The magnetic exchanges constants in MnO were also determined by analyzing a magnetic pair distribution function (mPDF) obtained by total neutron scattering measurements. The J_2/J_1 ratio of ∼1.5 was found to agree with the results of density functional theory (DFT) calculations.[16] While the results of the INS and mPDF analyses are slightly different, it is important to note that both methods revealed $J_2 > J_1$.

Given the higher covalency of the Mn−S bonds relative to that of the Mn−O bonds, it is of interest to investigate how the increased delocalization of bonding electrons affects the exchange constants in the AFM structure of MnS. Herein, we report the first INS study of the magnetic exchange interactions in MnS. The most striking observation is the large increase in the $|J_2/J_1|$ ratio (>3) for MnS as compared to the ratio of exchange parameters (∼1.5) reported for MnO. We use DFT calculations to support the modeling of the INS data. Furthermore, we demonstrate that the empirical U parameter used in the DFT calculations can lead to a broad variation of the J_1 and J_2 constants. Thus, the INS data provide a viable reference point to benchmark the DFT methods, while the latter provide a viable justification for conclusions drawn from the INS data.

MATERIALS AND METHODS

Synthesis of MnS. A bulk powder sample of MnS was prepared according to the published procedure.[17] A Teflon-lined vessel for solvothermal reactions was loaded with 245 mg of $Mn(OAc)_2{\cdot}4H_2O$ and 228 mg of thiourea ($C_2H_5N_5$), which were covered with 60 mL of ethanol. The solution was stirred for 30 min, after which the autoclave was sealed and maintained at 180 °C for 12 h. The product that precipitated was recovered by filtration, washed with ethanol, and dried under vacuum at 60 °C. Yield = 350 mg (74%). Several such samples were combined to obtain a multigram sample that was used in the neutron scattering experiments.

Magnetic Measurements. Measurements were carried out on the powder samples using a magnetic property measurement system (MPMS-XL, Quantum Design) equipped with a superconducting quantum interference device (SQUID). Direct-current (dc) magnetic susceptibility was measured in the temperature range of 1.8−300 K under an applied magnetic field of 100 Oe.

Powder X-ray Diffraction. Measurements were carried out at room temperature using a Panalytical X'Pert Pro diffractometer with an X'Celerator detector and Cu-Kα radiation source (λ = 1.54187 Å). The diffraction data were recorded in the 2θ range from 10 to 80° with a step of 0.05° and a total collection time of 1 h. The data analysis was carried out with HighScore Plus.[18]

Neutron Powder Diffraction. Neutron powder diffraction (NPD) experiments were carried out on the HB-2A high-resolution diffractometer of the High-Flux Isotope Reactor (HFIR) facility at the Oak Ridge National Laboratory (ORNL).[19] A sample of ∼3 g held in a cylindrical vanadium container was placed in a top-loading temperature-controlled system. The λ = 1.539 Å radiation was provided by a vertically focused Ge(115) monochromator. The data were collected by scanning the detector array consisting of 44 ^{3}He tubes, to cover the total 2θ range of 7−133° in steps of 0.05°. Overlapping detectors for a given step served to average the counting efficiency of each detector. Rietveld refinement of the collected data was carried out using FullProf.[20] An analysis of symmetry-allowed magnetic models was carried out using SARAh representational analysis software[21] and MAXMAGN at the Bilbao crystallographic server.[22]

Inelastic Neutron Scattering. INS measurements were carried out on the time-of-flight direct geometry spectrometer HYSPEC at the ORNL Spallation Neutron Source (SNS) facility. The HYSPEC measurements were carried out at 5, 100, 150, and 200 K with incident energy (E_i) of 30 meV, selected by a Fermi chopper with frequency of 300 Hz.

DFT Calculations. All calculations were run using the Vienna ab Initio Simulation Package (VASP)[23−25] with PAW-GGA pseudopotentials[26] being used for all elements in the high-precision mode. Atomic positions and cell parameters were used without geometry optimization. Calculations were run on the smallest primitive cell possible for each magnetic configuration (see the section "Analysis of Magnetic Exchange Interactions"). The following Γ-centered k-point grids were used for each magnetic configuration, attempting to maintain the same k-point density among different primitive cell sizes: FM, 15 × 15 × 15; AFM1, 15 × 15 × 11; AFM2, 10 × 10 × 10; AFM3, 15 × 15 × 15; AFM4, 11 × 11 × 15; AFM5, 15 × 15 × 5. All Mn atoms had their magnetic moments set to ±5 μ_B to initialize the desired magnetic configuration, with all O or S atoms starting with a magnetic moment of 0 μ_B. Initializing from the experimentally observed magnetic moments per Mn atom had no effect on the results of the calculations. For the calculations including the U parameter, the Mn atoms were given the desired U value, while the O and S atoms were given values of U = 0. All other settings were left unchanged from the VASP default settings.

https://doi.org/10.1021/acs.jpcc.1c02956
J. Phys. Chem. C 2021, 125, 16183−16190

RESULTS AND DISCUSSION

Synthesis and Magnetic Properties. A bulk sample of MnS, prepared according to the reported procedure,[17] was confirmed to be phase-pure by powder X-ray diffraction (Figure S1). The cubic unit cell parameter was in a good agreement with the previously reported value.[5] Magnetic measurements confirmed the AFM transitions at T_N = 152 K, which also agreed with the literature data[27−29] (Figure S2).

Magnetic Structure Determination. NPD experiments were carried out on the HB-2A diffractometer at ORNL. Examination of the NPD pattern of MnS recorded at 4 K (below T_N) revealed the presence of additional peaks that did not appear in the experimental NPD pattern recorded at 200 K (above T_N) or in the pattern calculated from the nuclear structure (Figure 2). This set of new peaks was successfully

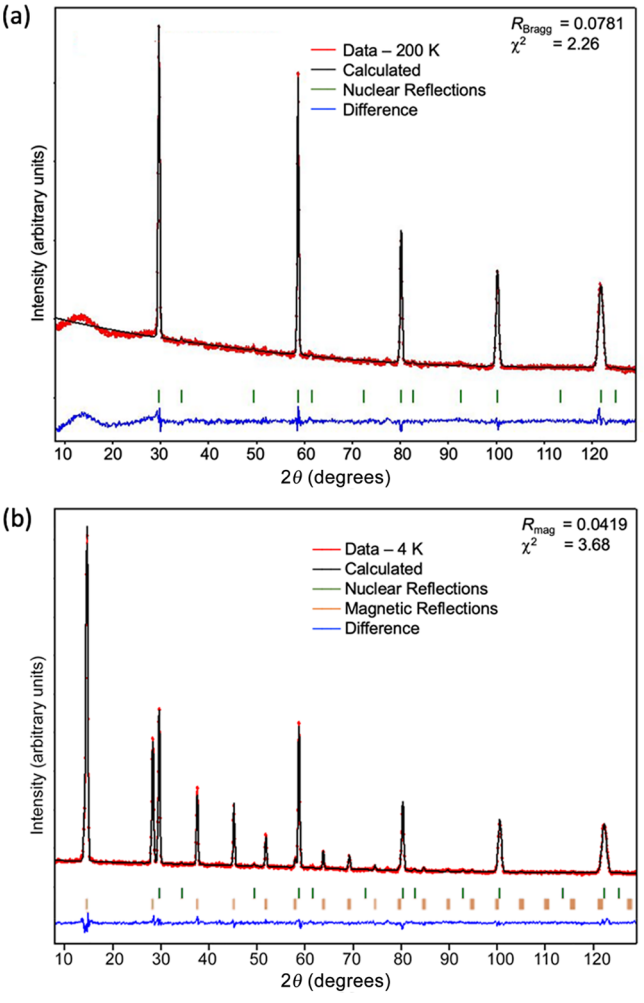

Figure 2. Results of Rietveld refinement of the experimental NPD patterns of MnS recorded at 200 K (a) and 4 K (b) in zero applied magnetic field.

indexed with the propagation vector $\boldsymbol{k}$ = (1/2, 1/2, 1/2). Thus, the volume of the magnetic unit cell of MnS is 8 times larger than the volume of its nuclear cell. These observations agree with the magnetic structure containing Mn moments that are FM coupled in the (111) lattice planes and aligned antiparallel (AFM) to the moments in adjacent planes of the (111) family (Figure 1). The magnetic structure is described by the magnetic space group C_c2/m (#12.63) in the unit cell base ($2\boldsymbol{a}$, $2\boldsymbol{b}$, $2\boldsymbol{c}$), relative to the nuclear unit cell base, ($\boldsymbol{a}$, $\boldsymbol{b}$, $\boldsymbol{c}$). Rietveld refinement (Table 1) of the NPD pattern recorded at

Table 1. Details of the Magnetic Structure Refinement Parameters for MnS[a]

temperature, K	4.0
wavelength, Å	1.537
magnetic space group	C_c2/c
magnetic unit cell parameter, $2\boldsymbol{a}$ (Å)	10.4056(1)
magn. moment (μ_B), m(Mn) = (m_a, 0, $-m_a$)	4.4(1)
R_p, R_{wp}	0.0353, 0.0464
R_{mag}	0.0419
χ^2	3.68

[a] $R_p = \sum|Y_o - Y_c|/\sum|Y_o|$; $R_{wp} = \sum[w(Y_o - Y_c)^2/\sum w(Y_o)^2]^{1/2}$; $R_{mag} = \sum|I_o - I_c|/\sum|I_o|$, where Y_o and Y_c are, respectively, the observed and calculated profile intensities taken with a 0.05° step and I_o and I_c are the corresponding intensities of magnetic peaks.

4 K resulted in a magnetic moment of 4.4(1) μ_B per Mn atom. This value is comparable to the previously reported values that were also established by NPD studies.[5,6] The Mn magnetic moment in MnS is notably smaller than the moment of 5.60 μ_B per Mn atom reported for MnO at 4.2 K.[30] The partial quenching of the moment in the MnS structure can be attributed to the increased covalency of Mn−S bonds as compared to Mn−O bonds.

Analysis of Magnetic Exchange Interactions. *Inelastic Neutron Scattering.* INS experiments were carried out using the HYSPEC spectrometer at the ORNL SNS facility. The INS technique offers a direct and quantitative measurement of the magnetic exchange interactions. An incident energy (E_i) of 30 meV was used to capture the full energy bandwidth of the magnetic excitation spectrum. The results of INS measurements are shown in Figure 3 as color-coded neutron scattering intensity maps of energy transfer versus momentum transfer (Q). The magnetic excitation spectrum measured at 5 K (Figure 3a) consists of a dispersive spin-wave excitation extending to approximately 15 meV. A shift of the spectral weight toward the low-energy region is observed at 100 K (Figure 3b). As the ordering temperature approaches 150 K, the excitations become weaker and less dispersive (Figure 3c). The inelastic excitations are still present but clearly diminished as the temperature is increased above T_N (Figure 3d).

The magnetic structure of MnS below T_N is well-defined as AFM; thus, the excitations may be modeled using the spin-wave theory according to the 3D Heisenberg model. A simple model accounting only for the NN (J_1) and next-NN (J_2) interactions was insufficient to provide a satisfactory fit to the experimental spectra. Therefore, additional parameters were introduced into the Hamiltonian eq 1, including the next-next-NN coupling constant (J_3) and the single-ion anisotropy parameter (D) with the direction defined by the unit vector $\hat{e}$:

$$\mathcal{H} = \sum_{<i,j>_{n=1,2,3}} J_n S_i S_j + \sum_i D(\hat{e}\cdot S_i)^2 \quad (1)$$

According to this Hamiltonian, the positive and negative values of J_n (Figure 4a) represent AFM and FM exchange couplings, respectively. This convention was used to allow a direct comparison to the modeling of INS data for MnO described in the earlier works.[13,14] We note that MnS does not exhibit a rhombohedral distortion at lower temperatures, in contrast to

https://doi.org/10.1021/acs.jpcc.1c02956
J. Phys. Chem. C 2021, 125, 16183−16190

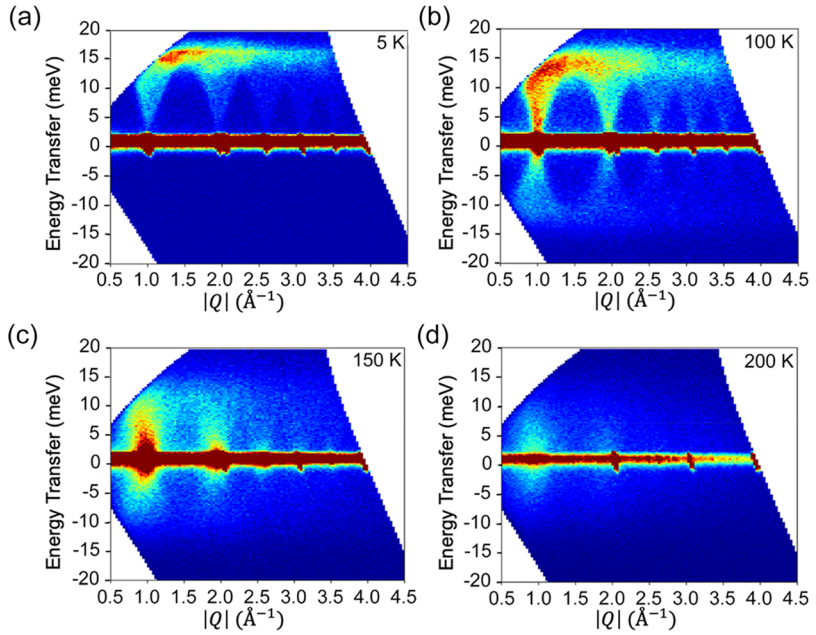

Figure 3. Contour plots of inelastic neutron scattering intensity measured on a powder sample of MnS at different temperatures using the incident energy of 30 meV.

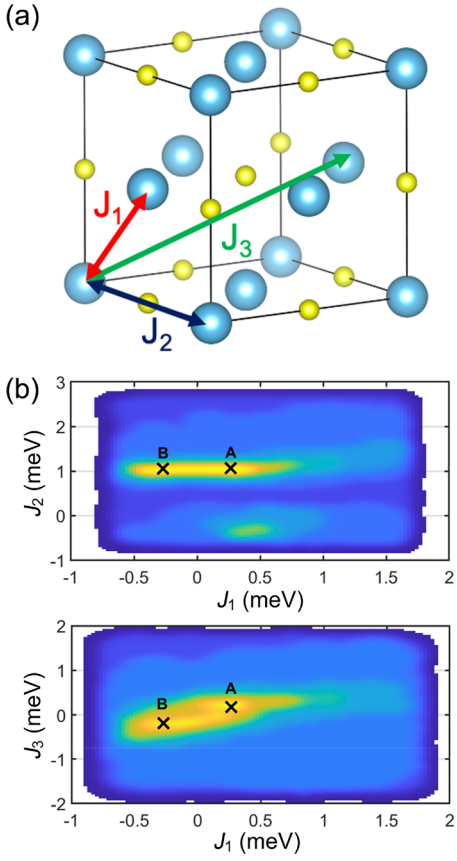

Figure 4. (a) Three magnetic interactions described by the exchange coupling constants J_1, J_2, and J_3 in the crystal structure of MnS. Color scheme: Mn = light-blue, S = yellow. (b) Contour plots showing the quality of fit to the INS experimental data for various values of the magnetic exchange constants. The yellow areas correspond to the optimal fit.

MnO, where such a distortion necessitated the introduction of two different NN exchange coupling constants, J_1^+ and J_1^-.

The powder averaged spin-wave excitations were calculated within the linear spin-wave theory using the SpinW package.[31] The easy-axis anisotropy was fixed at the value D = 0.03 meV reported in the literature,[32] oriented in a direction orthogonal to the $\boldsymbol{k}$-vector of the magnetic structure. Such small anisotropy, which was suggested to be due to dipolar interaction, is undetectable with our experimental configuration. The modeling of INS data consistently showed that the absolute value of J_1 should be substantially smaller than that of J_2 but larger than that of J_3. Considering the three independent parameters of the Hamiltonian space, we employed a machine learning technique for simultaneously extracting model solutions and estimating their uncertainty over a broad parameter space.[33] The cost function for the optimization process was:

$$X^2_{\mathrm{INS}} = \sum_{\omega,Q} m(Q,\omega)\,(S_{\mathrm{exp}}(Q,\omega) - S_{\mathrm{cal}}(Q,\omega))^2$$

where $m(Q,\omega)$ represents a step function to mask pixels out of detector coverage. A low-cost estimator of $\tilde{X}^2_{\mathrm{INS}}$, subjected to the constraint $\tilde{X}^2_{\mathrm{INS}} < c$, was used to evaluate the Hamiltonian parameters in an iterative process. The last iteration was attained when the cutoff (c) reached a value for which the calculated intensity agreed with the INS data within the experimental uncertainty. The manifold of possible parameter solutions is presented by contour plots in Figure 4b.

While the global AFM structure needs the dominant J_2 parameter to be positive, satisfactory fits to the experimental data could be obtained with both positive (AFM) and negative (FM) values of J_1 and J_3. As can be seen from Figure 4, the value of J_2 is well-localized near 1 meV, but the ratio J_2/J_1 is spread over a broad range ($3 < |J_2/J_1| < 6$) . Two representative solutions have been selected, corresponding to the parameters J_1 = 0.27 meV, J_2 = 1.06 meV, J_3 = 0.18 meV (all J_n couplings AFM) and J_1 = −0.27 meV, J_2 = 1.05 meV, J_3 = −0.19 meV (AFM J_2 and FM J_1 and J_3). These two solutions are indicated

https://doi.org/10.1021/acs.jpcc.1c02956
J. Phys. Chem. C 2021, 125, 16183−16190

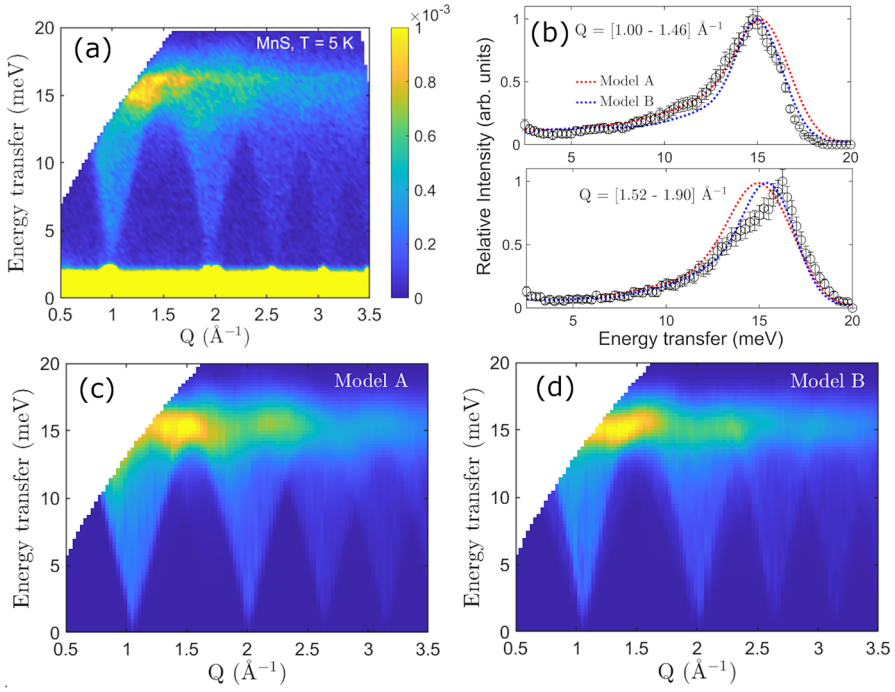

Figure 5. (a) INS data measured on a powder sample of MnS at 5 K. (b) Comparison of two selected model fits to the experimental data obtained for two Q-integrated regions, 1.00−1.46 Å^{-1} and 1.52−1.9 Å^{-1}. Models A and B correspond to $J_1 > 0$ (AFM) and $J_1 < 0$ (FM), respectively. The best-fit values are given in the text. (c, d) Calculated powder average spin-wave spectra, $S(Q, E)$, corresponding to models A and B.

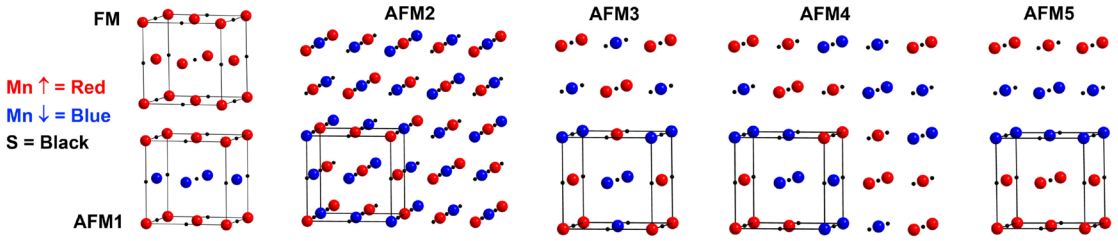

Figure 6. Spin configurations used for calculating the total energies and J_n values of MnS and MnO. The red and blue Mn atoms indicate different orientations of Mn magnetic moments. The nuclear unit cell is shown with solid black lines.

as "A" and "B" in Figure 4. The quality of fit of both models to the experimental data (Figure 5a) is shown in Figure 5b as cuts along the energy transfer axis taken over two Q-integrated regions. The calculated powder average spectra, $S(Q, E)$, corresponding to the two solutions are given in Figure 5c,d. We found that the relative quality of fit to the two models depended slightly on the Q-range over which the integration was taken, but overall, the scattering amplitude appeared to be well-matched by both models. To obtain an additional insight into the validity of these models, we carried out DFT calculations to determine the J_n values.

DFT Calculations. The total energy of a specific ground-state spin configuration (σ) can be expressed as a linear combination of the J_n values:[34−36]

$$E_{tot}(\sigma) = E_0 - \frac{\mu^2[\sigma]}{8} \sum_l \Delta z_l[\sigma] J_l \quad (2)$$

where E_0 is the total energy of the non-spin-polarized ground state, $\mu[\sigma]$ is the magnetic moment per atom, and $\Delta z_l[\sigma]$ is the difference between the number of FM and AFM interactions in the n^{th} coordination sphere of the central atom (considering only Mn atoms), given the configuration σ. Using eq 2 and the set of magnetic structures shown in Figure 6, the following system of equation is obtained:

$$E_{tot}(\mathrm{FM}) = E_0 - \frac{\mu^2[\sigma]}{8}(12J_1 + 6J_2 + 24J_3 + 12J_4 + 24J_5) \quad (3)$$

$$E_{tot}(\mathrm{AFM1}) = E_0 - \frac{\mu^2[\sigma]}{8}(-4J_1 + 6J_2 - 8J_3 + 12J_4 - 8J_5) \quad (4)$$

$$E_{tot}(\mathrm{AFM2}) = E_0 - \frac{\mu^2[\sigma]}{8}(-6J_2 - 12J_4) \quad (5)$$

$$E_{tot}(\mathrm{AFM3}) = E_0 - \frac{\mu^2[\sigma]}{8}(-4J_1 + 2J_2 + 8J_3 - 4J_4 - 8J_5) \quad (6)$$

$$E_{tot}(\mathrm{AFM4}) = E_0 - \frac{\mu^2[\sigma]}{8}(-2J_2 - 4J_4) \quad (7)$$

https://doi.org/10.1021/acs.jpcc.1c02956
J. Phys. Chem. C 2021, 125, 16183−16190

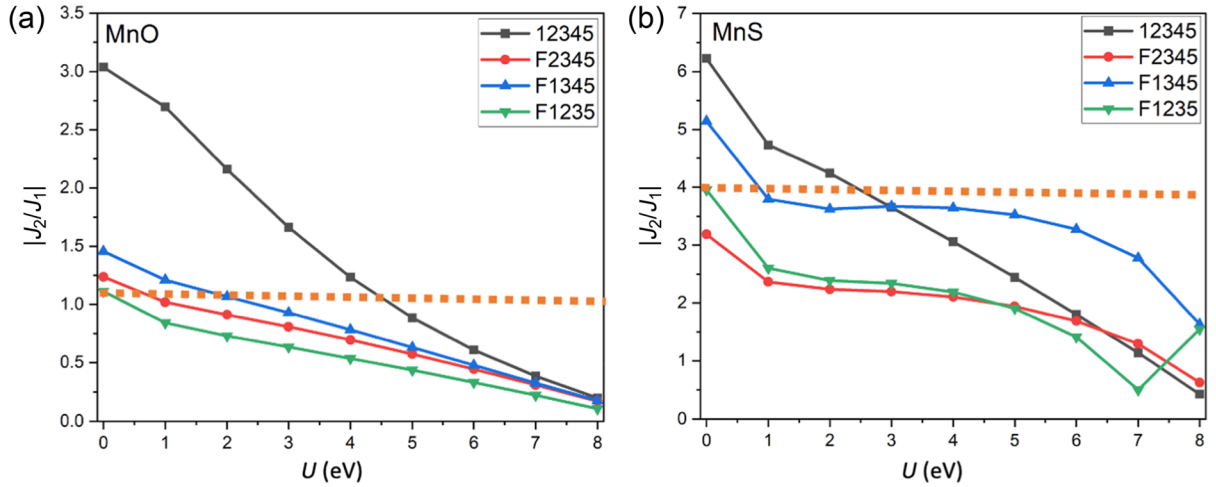

Figure 7. $|J_2/J_1|$ ratios calculated for MnO (a) and MnS (b) at various values of the parameter U. The sets of spin configurations used to calculate the J_n values from the system of eqs 3−8 are indicated in the legend, where F indicates the FM state and the numbers indicate different AFM states (Figure 6). The dotted horizontal lines indicate the $|J_2/J_1|$ ratios determined by fitting the experimental INS data.

$$E_{tot}(\text{AFM5}) = E_0 - \frac{\mu^2[\sigma]}{8}(4J_1 + 2J_2 - 8J_3 - 4J_4 + 8J_5) \quad (8)$$

We chose to use the larger number of magnetic configurations and exchange constants, as compared to the number of J_n values used in modeling of the experimental data, to allow for more statistically reliable values of the exchange constants extracted through this theoretical procedure.

Nevertheless, this theoretical approach is not without caveats. First, since the six chosen magnetic configurations create a degenerate set of linear equations, one of eqs 3−8 has to be omitted to allow an unambiguous solution of the system of equations. The decision which equation to omit is somewhat arbitrary. Second, the DFT method underestimates the localization of magnetic moments, necessitating the use of the empirical Hubbard parameter (U). In principle, the parameter can be adjusted to match the theoretical results to some experimental observation. For example, U can be varied until the AFM ordering temperature (T_N), calculated from the values of J_n through the mean-field theory, matches the experimentally observed value of T_N. Such an approach, however, is obviously problematic, since the mean-field theory is a rough approximation, especially in the case of competing magnetic interactions.

The availability of the experimental INS data provides a convenient reference point to address the problem with the choice of U. Since the modeling of experimental data led to the determination of the best ranges for the J_2/J_1 and J_1/J_3 ratios, the U value can be tuned to bring the ratios of the calculated exchange parameters closer to the best-fit ranges. Varying the value of U will affect the values of total energies obtained from the DFT calculations on specific spin configurations. The values of those energies enter the linear equations that define the values of J_i; therefore, the value of U influences indirectly the resulting values of J_i.

Using this strategy, we varied the value of U from 0 to 8 eV, calculating the total energies for all spin configurations σ shown in Figure 6. Configuration AFM2, which corresponds to the experimentally observed magnetic structure, was found to be the lowest-energy state for all values of U (Table S1), thus supporting the reliability of our calculation results. Next, a decision had to be made as to which configuration σ to exclude to solve the system of equations. It can be shown that excluding configurations AFM3 or AFM5 also leads to degenerate solutions. A comparison of the E_{tot} values as a function of U for all considered spin configurations showed that the FM state was always the highest in energy (Figure S3). Therefore, eq 3, defining the energy of this state, was omitted from the system of equations, and the solution for the J_n values was calculated at each value of U.

The J_n values showed gradual variation as a function of U (Figure 7 and Table S2). The optimal range of U was identified by comparing the J_2/J_1 and J_1/J_3 ratios obtained from calculations to the best-fit values of these ratios obtained from the analysis of experimental data (models A and B). To validate our theoretical approach, we also carried out the same calculations and analysis on MnO (Table S3 and Figure S4), for which the values of J_1 and J_2 had been established from the earlier INS studies.[37] We found that U = 4−5 eV gave the best agreement with the experimental data for MnO (Figure 7a), while U = 2−3 eV gave the best agreement for MnS (Figure 7b). Good agreements were achieved for both J_2/J_1 and J_1/J_3 ratios (Table 2).

Table 2. Comparison of Ratios $|J_2/J_1|$ and J_1/J_3 Obtained from Fitting the Experimental INS Data with Models A and B (Figure 5) and Calculated Based on the Total Energies of Five Spin Configurations (AFM1−AFM5 in Figure 6) as Functions of the U Parameter

ratio	$\|J_2/J_1\|$	J_1/J_3
model A	3.93	1.50
model B	3.89	1.42
Calculated from Configurations AFM1−AFM5		
U = 2 eV	4.244	1.028
U = 3 eV	3.650	1.124

The signs of J_n calculated without the FM model matched the ones obtained for model B. Interestingly, omitting one of the AFM configurations led to the signs of J_n matching model A. Importantly, however, omitting configuration AFM1, AFM2, or AFM4 consistently led to a large disagreement between the calculated and experimental J_1/J_3 ratios (Table

https://doi.org/10.1021/acs.jpcc.1c02956
J. Phys. Chem. C 2021, 125, 16183−16190

S2). Hence, we conclude that the signs and optimal values of J_n constants given by model B provide the best agreement between the experimental and theoretical results.

CONCLUDING REMARKS

This work presents the first detailed study of magnetic exchange interactions in MnS by a combination of INS spectroscopy and DFT calculations. Remarkably, we find that the next-NN exchange constant J_2, describing the interaction across the 180° Mn−S−Mn bridge, is more than 3 times larger than the NN exchange constant J_1, describing the combined direct exchange and the superexchange across the 90° Mn−S−Mn bridge. This is in contrast to MnO, which shows closer values of these constants, with $J_2/J_1 \leq 1.5$. Moreover, while both J_1 and J_2 in MnO correspond to AFM exchange coupling, in MnS they, likely, describe FM and AFM exchange couplings, respectively. While the INS data could be also modeled with the same sign for J_1 and J_2, the DFT calculations indicate that the model with different signs provides a better match to the experimental data.

From the magnetism point of view, two significant changes take place upon going from MnO to MnS: (1) The covalency of the metal−nonmetal bonding is increased, which is reflected in the suppression of the Mn magnetic moment. (2) The distance between the Mn sites is increased, which should weaken the direct Mn···Mn exchange interactions and increase the importance of the superexchange mediated by the bridging nonmetal atoms. These changes might help to justify the observed increase in the relative contribution from the J_2 exchange pathway in the magnetic structure of MnS, as well as the change in the sign of the J_1 exchange constant when going from MnO to MnS. The direct exchange was shown to play an important role in MnO,[38] and as such, it has a strong impact on the J_1 exchange constant. The increased NN Mn···Mn distance in MnS decreases the importance of the direct exchange contribution, while the Anderson superexchange mechanism becomes even more dominant due to the increased covalency. The relative changes in the J_1, J_2, and J_3 exchange constants and the competing nature of magnetic exchange interactions should also lead to different orientation of the Mn moments in the AFM-ordered structure of MnS as compared to the AFM-ordered structure of MnO.[3] Neutron scattering experiments on a single crystal of MnS can help to address this question and establish a more accurate model of magnetic exchange interactions. We are currently pursuing such research efforts, and the results will be reported in due course.

ASSOCIATED CONTENT

Supporting Information

The Supporting Information is available free of charge at https://pubs.acs.org/doi/10.1021/acs.jpcc.1c02956.

Powder X-ray diffraction, magnetic data, and details of the DFT calculations (PDF)

AUTHOR INFORMATION

Corresponding Authors

V. Ovidiu Garlea − *Neutron Scattering Division, Oak Ridge National Laboratory, Oak Ridge, Tennessee 37831, United States*; Email: garleao@ornl.gov

Michael Shatruk − *Department of Chemistry and Biochemistry, Florida State University, Tallahassee, Florida 32306, United States; National High Field Magnetic Laboratory, Tallahassee, Florida 32310, United States*; orcid.org/0000-0002-2883-4694; Email: mhatruk@fsu.edu

Authors

Judith K. Clark − *Department of Chemistry and Biochemistry, Florida State University, Tallahassee, Florida 32306, United States*

Vincent Yannello − *Department of Chemistry, Biochemistry and Physics, University of Tampa, Tampa, Florida 33606, United States*

Anjana M. Samarakoon − *Neutron Scattering Division, Oak Ridge National Laboratory, Oak Ridge, Tennessee 37831, United States;* Present Address: Materials Science Division, Argonne National Laboratory, Lemont, IL 60439, USA

Cyris Ross − *Department of Chemistry and Biochemistry, Florida State University, Tallahassee, Florida 32306, United States*

Madeleine C. Uible − *Department of Chemistry and Biochemistry, Florida State University, Tallahassee, Florida 32306, United States*

Complete contact information is available at: https://pubs.acs.org/10.1021/acs.jpcc.1c02956

Notes

The authors declare no competing financial interest.

ACKNOWLEDGMENTS

This research was supported by the National Science Foundation (award DMR-1905499 to M.S.). J.K.C. acknowledges the support by the Department of Energy SCGSR graduate fellowship. A portion of this research used resources at the High Flux Isotope Reactor and Spallation Neutron Source, DOE Office of Science User Facilities, operated by the Oak Ridge National Laboratory. This research also used resources provided by the X-ray Crystallography Center (FSU075000XRAY) and the Materials Characterization Laboratory (FSU075000MAC) at the FSU Department of Chemistry and Biochemistry.

REFERENCES

(1) Squire, C. F. Antiferromagnetism in some manganous compounds. *Phys. Rev.* **1939**, *56*, 922−925.

(2) Shull, C. G.; Strauser, W. A.; Wollan, E. O. Neutron diffraction by paramagnetic and antiferromagnetic substances. *Phys. Rev.* **1951**, *83*, 333−345.

(3) Goodwin, A. L.; Tucker, M. G.; Dove, M. T.; Keen, D. A. Magnetic structure of MnO at 10 K from total neutron scattering data. *Phys. Rev. Lett.* **2006**, *96*, 047209.

(4) Corliss, L.; Elliott, N.; Hastings, J. Magnetic structures of the polymorphic forms of manganous sulfide. *Phys. Rev.* **1956**, *104*, 924−928.

(5) Heide, H. v. d.; Bruggen, C. F. v.; Wiegers, G. A.; Haas, C. On the nature of the phase transitions in α-MnS. *J. Phys. C: Solid State Phys.* **1983**, *16*, 855−868.

(6) Huang, C.-H.; Wang, C.-W.; Chang, C.-C.; Lee, Y.-C.; Huang, G.-T.; Wang, M.-J.; Wu, M.-K. Anomalous magnetic properties in Mn(Se, S) system. *J. Magn. Magn. Mater.* **2019**, *483*, 205−211.

(7) Fender, B. E. F.; Jacobson, A. J.; Wedgwood, F. A. Covalency parameters in MnO, α-MnS, and NiO. *J. Chem. Phys.* **1968**, *48*, 990−994.

(8) Jacobson, A. J.; Fender, B. E. F. Covalency parameters in MnSe and $MnSe_2$. *J. Chem. Phys.* **1970**, *52*, 4563−4566.

(9) Franzen, H.; Sterner, C. The X-ray photoelectron spectra of MnS, MnSe, and MnTe. *J. Solid State Chem.* **1978**, *25*, 227−230.
(10) Pak, C.; Garlea, V. O.; Yannello, V.; Cao, H.; Bangura, A. F.; Shatruk, M. $Na_2Mn_3Se_4$: Strongly frustrated antiferromagnetic semiconductor with complex magnetic structure. *Inorg. Chem.* **2019**, *58*, 5799−5806.
(11) Bhutani, A.; Behera, P.; McAuliffe, R. D.; Cao, H.; Huq, A.; Kirkham, M. J.; dela Cruz, C. R.; Woods, T.; Shoemaker, D. P. Incommensurate magnetism in $K_2MnS_{2-x}Se_x$ and prospects for tunable frustration in a triangular lattice of pseudo-1D spin chains. *Phys. Rev. Mater.* **2019**, *3*, 064404.
(12) Clark, J. K.; Pak, C.; Cao, H.; Shatruk, M. Helimagnetism in $MnBi_2Se_4$ driven by spin-frustrating interactions between antiferromagnetic chains. *Crystals* **2021**, *11*, 242.
(13) Kohgi, M.; Ishikawa, Y.; Endoh, Y. Inelastic neutron scattering study of spin waves in MnO. *Solid State Commun.* **1972**, *11*, 391−394.
(14) Bonfante, M.; Hennion, B.; Moussa, F.; Pepy, G. Spin waves in MnO at 4.2 K. *Solid State Commun.* **1972**, *10*, 553−556.
(15) Morosin, B. Exchange striction effects in MnO and MnS. *Phys. Rev. B* **1970**, *1*, 236−243.
(16) Frandsen, B. A.; Brunelli, M.; Page, K.; Uemura, Y. J.; Staunton, J. B.; Billinge, S. J. L. Verification of Anderson superexchange in MnO via magnetic pair distribution function analysis and ab initio theory. *Phys. Rev. Lett.* **2016**, *116*, 197204.
(17) Biswas, S.; Kar, S.; Chaudhuri, S. Solvothermal synthesis of α-MnS single crystals. *J. Cryst. Growth* **2005**, *284*, 129−135.
(18) *X'Pert HighScore Plus Software* v. 2.2b; PANalytical B.V.: Almelo, Netherlands, 2006.
(19) Garlea, V. O.; Chakoumakos, B. C.; Moore, S. A.; Taylor, G. B.; Chae, T.; Maples, R. G.; Riedel, R. A.; Lynn, G. W.; Selby, D. L. The high-resolution powder diffractometer at the high flux isotope reactor. *Appl. Phys. A: Mater. Sci. Process.* **2010**, *99*, 531−535.
(20) Rodríguez-Carvajal, J. Recent advances in magnetic-structure determination by neutron powder diffraction. *Phys. B* **1993**, *192*, 55−69.
(21) Wills, A. S. A new protocol for the determination of magnetic structures using simulated annealing and representational analysis (SARAh). *Phys. B* **2000**, *276−278*, 680−681.
(22) Perez-Mato, J. M.; Gallego, S. V.; Tasci, E. S.; Elcoro, L.; de la Flor, G.; Aroyo, M. I. Symmetry-based computational tools for magnetic crystallography. *Annu. Rev. Mater. Res.* **2015**, *45*, 217−248.
(23) Kresse, G.; Hafner, J. Ab initio molecular dynamics for liquid metals. *Phys. Rev. B: Condens. Matter Mater. Phys.* **1993**, *47*, 558−561.
(24) Kresse, G.; Furthmüller, J. Efficiency of ab-initio total energy calculations for metals and semiconductors using a plane-wave basis set. *Comput. Mater. Sci.* **1996**, *6*, 15−50.
(25) Kresse, G.; Furthmüller, J. Efficient iterative schemes for ab initio total-energy calculations using a plane-wave basis set. *Phys. Rev. B: Condens. Matter Mater. Phys.* **1996**, *54*, 11169−11186.
(26) Kresse, G.; Joubert, D. From ultrasoft pseudopotentials to the projector augmented-wave method. *Phys. Rev. B: Condens. Matter Mater. Phys.* **1999**, *59*, 1758−1775.
(27) Banewicz, J. J.; Lindsay, R. Magnetic susceptibility of aMnS. *Phys. Rev.* **1956**, *104*, 318−320.
(28) Battles, J. W. Temperature dependence of the paramagnetic resonance linewidths in MnS and MnO. *J. Appl. Phys.* **1971**, *42*, 1286−1287.
(29) Huffman, D. R. Total intensities of some crystal field transitions in MnO and MnS related to the antiferromagnetism. *J. Appl. Phys.* **1969**, *40*, 1334−1335.
(30) Mellergård, A.; McGreevy, R. L.; Wannberg, A.; Trostell, B. Modelling of lattice and magnetic thermal disorder in manganese oxide. *J. Phys.: Condens. Matter* **1998**, *10*, 9401−9412.
(31) Toth, S.; Lake, B. Linear spin wave theory for single-Q incommensurate magnetic structures. *J. Phys.: Condens. Matter* **2015**, *27*, 166002.
(32) Chou, H. h.; Fan, H. Y. Light scattering by magnons in CoO, MnO, and α-MnS. *Phys. Rev. B* **1976**, *13*, 3924−3938.
(33) Samarakoon, A. M.; Barros, K.; Li, Y. W.; Eisenbach, M.; Zhang, Q.; Ye, F.; Sharma, V.; Dun, Z. L.; Zhou, H.; Grigera, S. A.; et al. Machine-learning-assisted insight into spin ice $Dy_2Ti_2O_7$. *Nat. Commun.* **2020**, *11*, 892.
(34) Johnston, D. C.; McQueeney, R. J.; Lake, B.; Honecker, A.; Zhitomirsky, M. E.; Nath, R.; Furukawa, Y.; Antropov, V. P.; Singh, Y. Magnetic exchange interactions in $BaMn_2As_2$: a case study of the J_1-J_2-J_c Heisenberg model. *Phys. Rev. B: Condens. Matter Mater. Phys.* **2011**, *84*, 094445.
(35) Uhl, M.; Siberchicot, B. A first-principles study of exchange integrals in magnetite. *J. Phys.: Condens. Matter* **1995**, *7*, 4227−4237.
(36) Eggert, S. Accurate determination of the exchange constant in Sr_2CuO_3 from recent theoretical results. *Phys. Rev. B: Condens. Matter Mater. Phys.* **1996**, *53*, 5116−5118.
(37) Kohgi, M.; Ishikawa, Y.; Harada, I.; Motizuki, K. Spin waves in manganese monoxide. *J. Phys. Soc. Jpn.* **1974**, *36*, 112−122.
(38) Harrison, W. A. Heisenberg exchange in the magnetic monoxides. *Phys. Rev. B: Condens. Matter Mater. Phys.* **2007**, *76*, 054417.

https://doi.org/10.1021/acs.jpcc.1c02956
J. Phys. Chem. C 2021, 125, 16183−16190